Journal of Photochemistry & Photobiology, B: Biology 153 (2015) 445–454

Contents lists available at ScienceDirect

Journal of Photochemistry & Photobiology, B: Biology

journal homepage: www.elsevier.com/locate/jphotobiol

Riboflavin acetate induces apoptosis in squamous carcinoma cells after photodynamic therapy

Andrea V. Juarez [a,*], Liliana del V. Sosa [a], Ana L. De Paul [a], Ana Paula Costa [b], Marcelo Farina [b], Rodrigo B. Leal [b], Alicia I. Torres [a], Patricia Pons [a]

[a] Centro de Microscopía Electrónica, Instituto de Investigaciones en Ciencias de la Salud (INICSA-CONICET), Facultad de Ciencias Médicas, Universidad Nacional de Córdoba, Ciudad Universitaria, 5000 Córdoba, Argentina

[b] Departamento de Bioquímica, Centro de Ciências Biológicas, Universidade Federal de Santa Catarina, Campus Universitário, 88040-900 Florianópolis, Santa Catarina, Brazil

ARTICLE INFO

Article history:
Received 4 May 2015
Received in revised form 26 October 2015
Accepted 31 October 2015
Available online 2 November 2015

Keywords:
Photodynamic therapy
SCC-13 cells
Riboflavin 2′,3′,4′,5′-tetraacetate
Apoptosis

ABSTRACT

Several research efforts have been focused on finding newer and more efficient photosensitizers for photodynamic therapy (PDT). Although, it was demonstrated that riboflavin is an efficient photosensitizer for PDT, the effect of its ester derivate, riboflavin 2′,3′,4′,5′-tetraacetate (RFTA), which has higher cellular uptake, has not been well defined. To evaluate the cell death generated by applying RFTA as the photosensitizer in PDT in a human cancer cell line of squamous carcinoma (SCC-13), these cells were incubated with riboflavin and its ester derivate, RFTA followed by irradiation with different blue light doses. Cell viability was evaluated using neutral red uptake assay and cell death was evaluated using transmission electron microscopy, TUNEL assay and annexin V-PE/7AAD double staining. The expression of caspase-3, Bax, Bcl-2, ERK 1/2 and $p38^{MAPK}$ was evaluated by Western blotting and generation of intracellular ROS and changes in anion superoxide levels were analyzed using 2′,7′-dichlorofluorescein-diacetate and dihydroethidium dye, respectively. RFTA-PDT generated a decrease in cancer cell viability in a light dose–response. Treated SCC-13 cells exhibited chromatin condensation, formation of apoptotic bodies, increases in TUNEL-positive cells, phosphatidylserine externalization and decreased procaspase-3 and Bcl-2 protein expression and increment of ERK 1/2 phosphorylation. Moreover, trolox abolished the effect of PDT on cell viability linking the increase in intracellular ROS levels with the cell death observed, whereas that the pre-treatment with MEK inhibitor did not induce changes in SCC-13 cell survival. These findings demonstrate the effects of RFTA in triggering apoptosis induced by ROS ($\bullet\backslash O_2^-$) production after visible light irradiation of squamous carcinoma cells.

1. Introduction

Photodynamic therapy (PDT) is an efficient clinical approach employed for treatment of non-melanoma cutaneous cancer including basal cell carcinoma and squamous cell carcinoma (SCC) [1,2]. PDT consists of three elements: a photosensitizer (Ps) (which is a compound applied topically or administered systemically), light (usually in the visible range) and molecular oxygen [3]. Although, each component is harmless by itself, together they can generate reactive oxygen species (ROS) following the absorption of visible light by a Ps. Subsequently, ROS are selectively accumulated into tumor cells, thereby inducing oxidative cell damage and cell death [4]. The cell death triggered after PDT varies according to the physical properties of the Ps employed, the light wavelength, PDT dose and cell type [5,6].

In recent years, new compounds with PDT applications have been developed [7]. However, only a few Ps including α-aminolevulinic acid (ALA) and its methyl ester derivative have been approved for use in clinical assays and in the treatment of some diseases, such as precancerous cutaneous lesion and non-melanoma skin cancer [8]. In this regard, new photosensitizers with PDT applications are currently being evaluated in an attempt to improve photophysical and photobiological properties [9,10]. Riboflavin (RF), known as vitamin B2, has been described to play an important biological role as a photochemical sensitizer, as it participates in numerous biological oxidation reduction reactions of a wide range of substrates [11,12]. When RF is photoactivated by visible radiation and in the obtained triplet-excited state, it can interact directly with a substrate to generate radical intermediates and ROS such as superoxide anion, hydroxyl radical and hydrogen peroxide. In addition, photoactivated RF can transfer energy to molecular oxygen, thus generating singlet oxygen by a different mechanism [12,13]. In fact, the use of RF in PDT has been described as an efficient inductor of several processes such as cell death, ROS production, as well as MAPK activation [14–18]. However, due to the hydrosoluble profile of RF, its incorporation in various tissues is low; therefore many studies have used RF ester derivatives with higher hydrophobicity in an attempt to

* Corresponding author.
E-mail address: virginiaajuarez@gmail.com (A.V. Juarez).

http://dx.doi.org/10.1016/j.jphotobiol.2015.10.030
1011-1344/

increase bioavailability [15]. In particular, the riboflavin 2′,3′,4′,5′-tetraacetate (RFTA) retains the photosensitizing properties of RF [19], exhibiting nearly identical absorbance spectra [20]. Thus the present study was focused on the ability of RFTA to promote a higher cellular uptake to provide a significant photochemical activity.

PDT provokes cell death through various mechanisms [21,22], which can be classified according to different criteria: morphological appearance, enzymatic features, immunological characteristics, and functional aspects [23]. It is well known that necrosis is accompanied by the progressive loss of the cytoplasmic membrane integrity, leading to local inflammation [24,25]. On the other hand, some lines of evidence indicate that PDT-induced cell death (mainly through apoptotic events) is devoid of inflammation, as has been observed in many tumor cell lines after PDT for different photosensitizers [26,27]. The molecular mechanism of apoptosis may involve various signaling pathways and is dependent of the modulation of a variety of proteins including mitogen activated protein kinases (MAPKs) [28]. Notably, the activation of MAPKs by PDT has been reported in several cell lines using different photosensitizers [29,30]. However, it is still unknown whether the activation of MAPKs can be triggered after PDT using RF or RFTA.

Taking into account the above finding, we took advantage of a human cancer cell line of squamous carcinoma (SCC-13) to evaluate the potential occurrence of cell death induced by RFTA-based PDT, as well as to elucidate potential mechanisms. Given that the PDT is a clinical approach employed to treat non-melanoma cutaneous cancer, we hypothesize that RFTA could also be applied to treat shallow skin lesions such as SCC in situ.

2. Materials and Methods

2.1. Photosensitizers

The photosensitizers used in this study were RF (Sigma-Aldrich, St. Louis, USA) and RFTA, which was obtained as previously described [19] with modification of the synthetic procedure [31]. Briefly, 0.5 g of RF was mixed with 100 mL of $(CH_3CO)_2O$:$C_2H_4O_2$ (1:1), and then 1 mL of $HClO_4$ was added and the mixture was refluxed for 3 h at 40 °C. The reaction was cooled to 0 °C, after 200 mL of cold deionizer water was added and extracted three times with 25 mL $CHCl_3$. The organic phase was washed with 25 mL of cold water followed by 25 mL of a cold saturated NaCl solution. The solvent was evaporated at 50 °C and the product recrystallized four times in CH_3OH:H_2O (17:3). Finally, RFTA was diluted in 1% (*v*/*v*) acetone–high glucose Dulbecco's modified Eagle's minimal essential medium (DMEM; Sigma-Aldrich, St. Louis, USA).

2.2. Cell Culture

The human cell lines SCC-13 obtained from SCC of the facial epidermis [32], and HaCaT an immortalized line of human epidermal keratinocytes were generously supplied by Universidad Nacional de Río Cuarto, Córdoba, Argentina. The SCC-13 and HaCat cells were cultured in DMEM supplemented with 1% of glutamine, penicillin 100 units/mL, streptomycin 10 mg/mL (Sigma-Aldrich, St. Louis, USA), 10% fetal bovine serum (FBS; Gibco), and 1% of sodium pyruvate 100 mM (Invitrogen, Carlsbad, CA). These cultures were maintained at 37 °C in a humidified atmosphere of 5% CO_2 and 95% air. Cells were cultured for 3 days with a confluence of 70%, and then submitted to different experimental protocols.

2.3. Photodynamic Treatment

SCC-13 cells were treated with RF and RFTA (50–200 μM) for 3 h to determine the non-toxic dose for the Ps. Next, cells were irradiated by employing a monochromatic light source (446 nm) with a multi-LED system (incoherent light) at irradiation doses of 4.5, 9 and 18 J/cm^2, and then maintained in DMEM containing 10% serum for 6, 12 or 24 h.

2.4. Cell Viability Assay

To analyze the Ps uptake by the HaCat and SCC-13 lines, cells were incubated with RF and RFTA for 3 h and the fluorescence intensity was evaluated by flow cytometry (FaCScan; Ortho Diagnostic System, Raritan, NJ) with an Ar-ion 488 nm laser for the excitation of green fluorescence, and data analysis was carried out using FlowJo software (Tree Star, Inc. Ashland, OR). A neutral red uptake assay was used to determine cell viability. After 24 h of treatment, the HaCat and SCC-13 cells were incubated with 0.08% neutral red (Merck KGaA, Darmstadt, Germany) for 2 h at 37 °C, and then washed with phosphate-buffered saline (PBS). The dye incorporated by viable cells was eluted by incubating with cold solubilization buffer (50% ethanol 96%; 49% deionized water, 1% glacial acetic acid) for 10 min. The optical density was measured at 540 nm, and the cell viability was calculated based on the difference of the optical density between the treatment and control group. The values obtained from control cultures were recorded as representing 100% of cell viability, and the results of the treatment were expressed as a percentage of these control cell values. Additionally, in order to inhibit the ROS production, cells were pre-treated with the antioxidant Trolox (20 μM, Sigma-Aldrich, St. Louis, USA) for 3 h before PDT. Also, with the aim to evaluate ERK 1/2 participation, the MEK inhibitor PD 098059 (50 μM, Sigma-Aldrich, St. Louis, USA) for 1 h before PDT was used.

2.5. SCC-13 Cell Proliferation

Immunocytochemical detection of bromodeoxyuridine (BrdU) was used to label the proliferating cells in the S-phase of the cell cycle. After 24 h of the treatment, the cells were incubated with BrdU (3 mg/mL) for 3 h. Then, cells attached to the glass coverslips were fixed with 4% formaldehyde for 30 min at room temperature (RT), washed in PBS, and permeabilized with 0.5% Triton X-100 for 10 min. Non-specific immunoreactivity was blocked with 1% PBS–BSA for 30 min at RT, and the cells were incubated overnight with a monoclonal antibody against BrdU (Amersham; Buckinghamshire, England) at 4 °C in a wet chamber. After that, the cells were incubated with biotinylated anti-mouse IgG diluted 1:100 for 30 min at RT (GE Healthcare; Buenos Aires, Argentina). The coverslips were washed with PBS and then incubated with avidin–biotin peroxidase complex (ABC; Vector; Burlingame, USA). Immunoreactivity for BrdU was visualized with 3,3-diaminobenzidine tetrahydrochloride (DAB) as a chromogen. A total of 1000 cells were examined in randomly chosen fields of each glass slide, in order to establish the percentage of immunoreactive cells for BrdU. Three coverslips were analyzed for each group, derived from the same cell preparations. The coverslips were then mounted on glass slides with glycerol, with controls having the same protocol applied, but omitting the BrdU antibody.

A total of 1000 cells were examined by light microscopy in randomly chosen fields of each coverslip, in order to establish the percentage of immunoreactive cells for BrdU. Three coverslips were analyzed for each group, derived from the same cell preparations. Experiments were replicated at least three times with separate batches of cell preparations.

2.6. Morphological Changes

The cells attached to the glass coverslips were incubated with RF or RFTA for 3 h, before being irradiated with 4.5 or 9 J/cm^2. After 12 or 24 h, cells were fixed with 4% formaldehyde for 30 min at RT, permeabilized with 0.5% Triton X-100 for 10 min, and stained with 200 μM Hoechst33258 (Molecular Probes) for 10 min at RT. Finally, the cells were observed using a Zeiss Axiovert 135 fluorescence microscope.

2.7. Ultrastructural Analysis

After 24 h of the treatments, SCC-13 cells were detached with TrypLE™ Express, washed, and centrifugated at 1000 rpm for 3 min. Then, the pellets were fixed by immersion in Karnovsky mixture containing 2% (*v*/*v*) glutaraldehyde and 4% (*v*/*v*) formaldehyde in 0.1 M cacodylate buffer plus 7% sucrose. After fixation, cells were washed with 0.1 M cacodylate buffer and post-fixed with 1% osmium tetroxide (Sigma-Aldrich, St. Louis, USA) in the same buffer for 1 h. Subsequently, the pellets were dehydrated in a graded acetone series and embedded in Araldite resin (Electron Microscopy Sciences, Hatfield, PA). Thin sections were cut with a diamond knife on a JEOL JUM-7 ultramicrotome (Nikon, Tokyo, Japan), stained with uranyl acetate and lead citrate, and examined using a Zeiss LEO 906-E electron (Oberkochen, Germany).

2.8. In Situ Detection of DNA Fragmentation

The apoptotic nature of cell death was confirmed by TUNEL using an In Situ Cell Death Detection Kit (POD; Roche Molecular Biochemicals, Mannheim, Germany), following the steps recommended in the manufacturer's instructions. Briefly, SCC-13 cells attached to the glass coverslips were fixed with 4% formaldehyde and permeabilized with 0.1% Triton X-100 for 2 min on ice. Cells were then incubated with a reaction mixture containing biotinylated nucleotides and terminal deoxynucleotidyl transferase (TdT) at 37 °C for 1 h. After incubation with the converter-POD solution for 30 min at 37 °C, the substrate DAB was added, and observations were made microscopically (Zeiss Axiostar plus). At least 20 randomly selected microscopic fields were examined with images obtained using an Axiocam ERc5s Zeiss digital compact camera. The percentage of TUNEL positive cells was calculated by counting at least 3000 cells per culture for at least three independent cell cultures.

2.9. Analysis of Apoptosis by Flow Cytometry

Following PDT, cells were collected from the monolayer with TrypLE™ Express. To detect phosphatidylserine externalization, SCC-13 were suspended in 200 μL binding buffer (100 mM HEPES, pH 7.4, 140 mM NaCl, 2.5 mM $CaCl_2$). The apoptotic analysis was performed using annexin V-PE and 7AAD according to the manufacturer's instructions (BD Pharmingen, USA). After 15 min of annexin V incubation at RT in darkness, 7AAD was added to the samples. Finally, the samples were analyzed by flow cytometry.

2.10. Western Blot Analysis

For the quantification of protein expression, Western blot analysis was performed as previously described [33]. The cultured cells SCC-13 were lysed with SDS-stopping solution (4% SDS, 2 mM EDTA, and 50 mM Tris, pH 6.8), and the lysates were boiled for 5 min and then centrifuged (10,000 ×*g* at 4 °C for 10 min). Protein content was estimated by Lowry assay. The same amount of protein (50 μg per lane) for each sample was electrophoresed in 10% SDS-PAGE minigels, before being transferred to nitrocellulose membranes using a semidry blotting apparatus (1.2 mA/cm^2; 1.5 h). The membranes were blocked with 5% bovine albumin (BSA) in Tris-buffered saline (TBS) (10 mM Tris, 150 mM NaCl, pH 7.5), and the targets were detected after overnight incubation with specific antibodies diluted in TBS with tween (TBS-T) that contained 2% BSA in a 1:1000 dilution of anti-Bax, anti-Bcl-2 (Biolegend, St. Diego, CA, USA) and anti-caspase-3 (Santa Cruz, CA, USA); 1:2000 anti-phospho ERK 1/2 (Sigma-Aldrich, St. Louis, USA); 1:10,000 anti-phospho p38^{MAPK}(Millipore, Billerica, MA, USA) and total-p38^{MAPK}, and 1:40,000 anti-total-ERK 1/2 (Sigma-Aldrich, St. Louis, USA). Membranes were incubated for 1 h at RT with horseradish peroxidase (HRP)-conjugated anti-rabbit or anti-mouse secondary antibodies (Millipore, Billerica, MA, USA) to detect the phosphorylated sites or the total form of the targets, with reactions being developed using chemiluminescence substrate (LumiGLO, Cell Signaling Technology, Beverly, MA, USA). All of the incubation steps were followed by washing three times with TBS-T (10 mM Tris, 150 mM NaCl, 0.1% Tween-20, pH 7.5). Each membrane was incubated with anti-β-actin antibody (1:2000; Santa Cruz, CA, USA) to verify that equal amounts of protein for each sample were loaded into the gel. The phosphorylation level was determined as a the ratio of the optic density (OD) of the phosphorylated band and the OD of the total band, with the bands being quantified using Scion Image® software, which is a derivative of NIH Image (Frederick, MD, USA). All other reagents were of analytical grade.

2.11. Reactive Species Detection

Intracellular reactive species (RS) production was detected using CM-H_2DCFDA (Invitrogen, USA), according to the manufacturer's instructions. Briefly, tumor cells were incubated with 50 μM RF or RFTA for 3 h, and for the last hour cells were exposed to dye (2.7 μM) at 37 °C in darkness to allow the incorporation and activation of the dye. Then, irradiation was performed with different doses (4.5 or 9 J/cm^2), and the free dye was removed. After 2 h of incubation, attached cells were visualized and photographed using a fluorescence microscope or harvested with TrypLE™ Express (Gibco, New York, USA) for analysis by flow cytometry. The mean fluorescence intensity was used as an index of the ROS level.

2.12. Superoxide Anion Generation

Superoxide anion ($\bullet O_2^-$) cytoplasmic production from PDT in SCC-13 cells was determined by using fluorescent dye dihydroethidium (DHE; Sigma, St. Louis, Mo). This assay is based on the reduction of ethidium by a O_2^- to a fluorescent compound [34]. After 6 h of RF or RFTA-PDT, cells were incubated with 10 μM DHE in HBSS for 30 min at 37 °C in darkness. After being rinsed with HBSS, the DHE fluorescence intensity in 24-well plates was measured with excitation at 488 nm and an emission at 585 nm, using a fluorimetric microplate reader (TECAN Group Ltd., Grödig, Austria).

2.13. Statistical Analysis

The statistical analysis was carried out using three replicates measured from three independent cell cultures. Data were analyzed using GraphPad Prism version 5.00 for Windows (GraphPad Software, San Diego, CA). A Student's t-test and a one-way ANOVA followed by the Tukey post-hoc test were performed for statistical analyses. Alternatively, treatments vs. light intensity, or cell type vs. treatment vs. light intensity interactions were analyzed by two or three-way ANOVA followed by the Bonferroni post-hoc test. Results are expressed as mean ± S.E.M. and the differences were considered significant when $p < 0.05$.

3. Results

3.1. SCC-13 Cell Viability Mediated by Photosensitizers With or Without Irradiation

The UV–visible spectra of the RF and RFTA for the SCC-13 cells cultured in DMEM complete medium, exhibited a peak at 374–371 and in the blue visible region at 446–447 nm, respectively (Fig. 1A). In addition, the uptake of RF and RFTA by HaCat and SCC-13 cells was analyzed, the results indicated that, in HaCat cells, the maximum fluorescence intensity (MFI) did not shift after RF and RFTA incubation, while in tumoral cells an increase in MFI was detected after photosensitizer treatment, suggesting a higher uptake of PS in SCC-13 cells (Fig. 1B). Next, to determine the effect of the photosensitizers on SCC-13 cell viability, the neutral red uptake colorimetric assay was carried out. SCC-13 cells

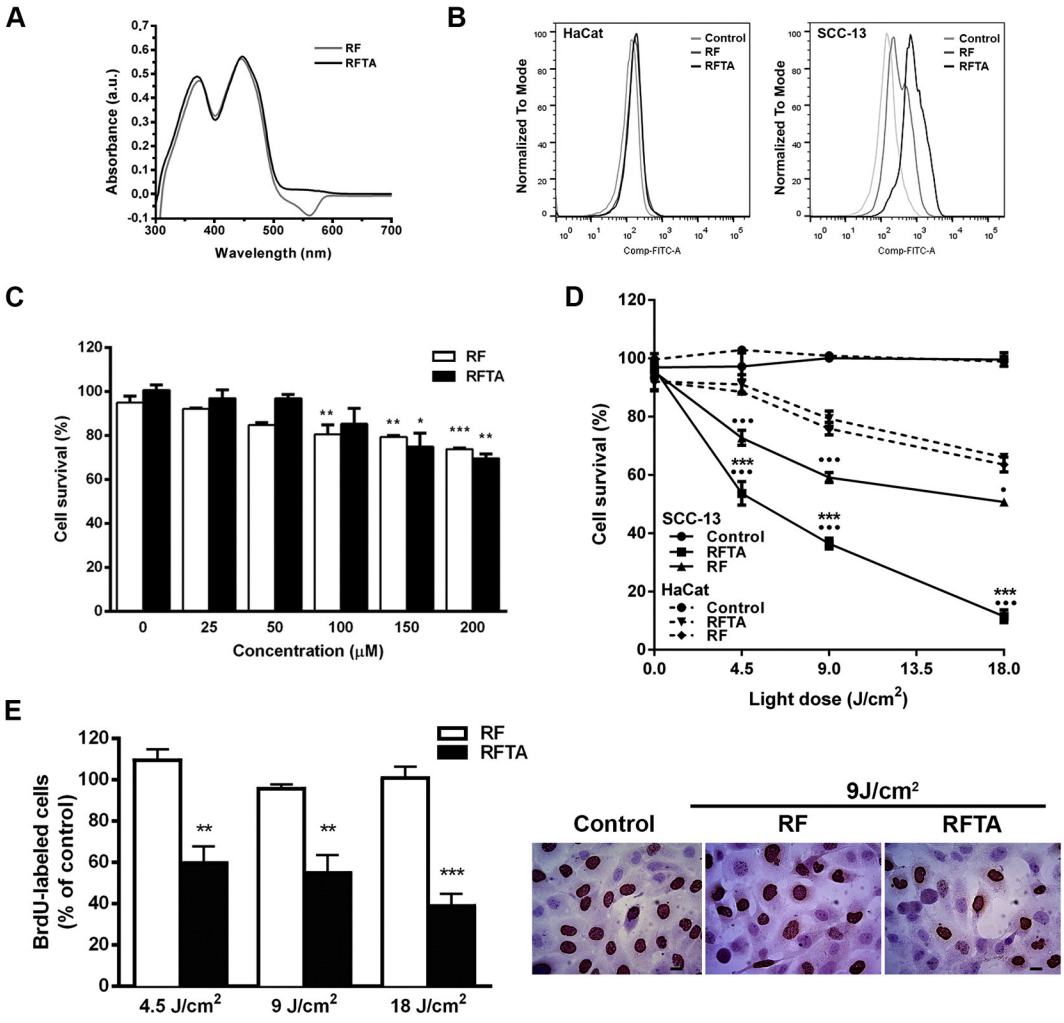

Fig. 1. Cell viability mediated by photosensitizers with or without irradiation. (A) Absorbance spectra from 300 nm to 700 nm of RF and RFTA in DMEM culture medium (50 μM) at pH 7.4. (B) Photosensitizer uptake by HaCat and SCC-13 cells after 3 h of incubation. (C) PS dose–response curve of SCC-13 cell viability after RF and RFTA incubation in darkness (*$p < 0.05$; **$p < 0.01$ and ***$p < 0.001$, vs. control). (D) Light dose-dependent effect on HaCat and SCC-13 cell survival after RF and RFTA incubation (50 μM) followed by blue irradiation. Data are represented as cell survival % of control and expressed as mean ± S.E.M. Two or three-way ANOVA, followed by Tukey post-hoc test (···$p < 0.001$ RF or RFTA in SCC-13 cells vs. HaCat cells; ***$p < 0.001$ RFTA vs. RF in SCC-13 cells). (E) Quantification and representative microphotograph of BrdU uptake (nucleus in brown) in control and treated cells. Data are expressed as number of BrdU-labeled cells (% of control: absence of PS and light exposure). Two-way ANOVA, treatment (RF vs. RFTA) [$F_{1,25} = 57.88$; $p < 0.0001$]. Bonferroni post-hoc test: **$p < 0.01$ and ***$p < 0.001$ RFTA vs. RF at the same light intensity condition. (For interpretation of the references to color in this figure legend, the reader is referred to the web version of this article.)

were incubated with RF or RFTA at different concentrations (25, 50, 100, 150 and 200 μM) for 3 h in darkness. As shown in Fig. 1C, neither RF nor RFTA at a low concentration (50 μM) caused a significantly decrease in cell viability. However, when the cells were incubated with RF or RFTA at a high concentration (150 μM), cell survival decreased by 20.7% ± 0.75 and 25.02% ± 6.03, respectively, compared to control. Therefore, based on this cell viability concentration-dependent, the dose of 50 μM was selected for further experiments.

In order to evaluate the effect of the Ps on the cell viability after irradiation, SCC-13 and HaCat cells were incubated with RF or RFTA (50 μM) for 3 h, followed by irradiation with a light dose ranging from 4.5 to 18 J/cm^2. As shown in Fig. 1D, there was a significant interaction between treatment and light intensity [two-way interaction: $F_{6,60} = 52.37$; $p < 0.001$] as well as between cell type, treatment and light intensity [three-way interaction: $F_{6,60} = 16.34$; $p < 0.001$], indicating that the hazardous effects of increasing light intensities, which are dependent on treatments (control, RF or RFTA), were significantly different between the two cell types. The HaCat and SCC-13 cell survival percentages diminished significantly in a light-dose dependent manner for both Ps, compared to control. As expected, the decrease in SCC-13 cell survival was more remarkable than in HaCat cells, indicating that tumoral cells were more sensitive to PDT. In addition, in SCC-13 cells, RFTA-PDT was more effective in decreasing cell survival when compared to RF treatment (Fig. 1D).

Considering that PDT applied to SCC-13 cells induced a decrease in cell viability, the proliferative rate (uptake of BrdU) was analyzed. After RFTA-PDT treatment, a decrease in the uptake of BrdU percentage of SCC-13 cells was observed for all light doses employed (Fig. 1E). These results clearly indicate that RFTA presented a higher capacity for decreasing cell proliferation than RF, regardless of the light intensity.

3.2. Characterization of Cell Death by Morphological Features

To determine whether the decrease in cell viability induced by PDT was caused by an increase in apoptosis, the morphological features were analyzed. SCC-13 cells were incubated with RF or RFTA (50 μM–3 h), irradiated with 9 or 18 J/cm^2 and incubated for an additional 24 h. Non-irradiated cells exhibited morphological characteristics similar to control cells whereas for irradiated tumoral cells after RF or RFTA exposure, nuclei with apoptotic characteristics such as clumps of hypercondensed chromatin and nuclei fragmentation were observed (Fig. 2A).

In order to explore the ultrastructural morphological changes triggered after treatments, SCC-13 cells were examined by TEM (Fig. 2B).

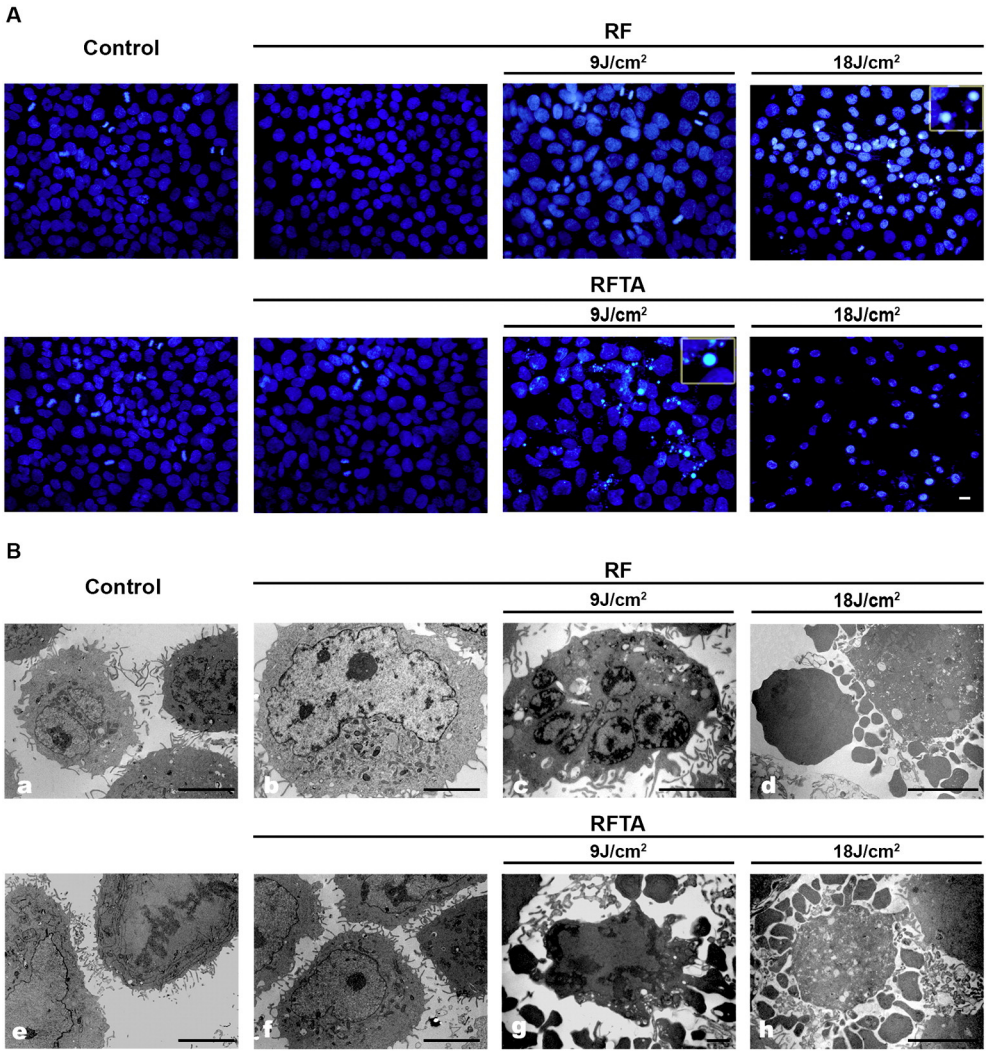

Fig. 2. Morphology of SCC-13 cells. (A) Representative micrographs from control and PDT-treated cells showing morphological nuclear changes by fluorescence microscopy; Inset: apoptotic cells. Scale bar: 8 μm. (B) Transmission electron micrograph of SCC-13 cells. Control cells in normal media (a and e) and non-irradiated cells treated with RF (b) or RFTA (f). Cells treated with RF-irradiation 9 J/cm^2 (c), 18 J/cm^2 (d), RFTA-irradiation 9 J/cm^2 (g) or 18 J/cm^2 (h). Scale bar: 2 μm.

The RF or RFTA treatments were unable to induce any modifications at the plasmatic or nuclear membranes when irradiation was omitted, similar to control cells. However, after PDT with RF (9 and 18 J/cm^2) or RFTA (9 J/cm^2), the cells exhibited alterations at the nucleus and cytoplasm, showing a progressive nuclear membrane disruption and condensed chromatin at the nuclear periphery, as well as the formation of apoptotic bodies. In addition, some RFTA-treated cells exposed to 18 J/cm^2 also showed the development of clear small cytoplasm vacuoles, dilated organelles and the progressive loss of the cytoplasmic membrane integrity, characteristics similar to those in necrotic cells (Fig. 2B-h). For this reason, the dose of 9 J/cm^2 was selected in the following assays to evaluate apoptotic cell death.

3.3. Apoptotic Cell Death Induced by PDT

To complement the study of apoptosis performed by morphological approaches, flow cytometry analysis of the annexin V-PE and 7AAD markers was carried out. As shown in Fig. 3A, in control cells apoptosis values of 5.38% and 4.87% corresponded to the early and late stages of apoptosis, respectively, with similar results being observed in RF-treated cells after PDT. However, in RFTA-exposed cells which were irradiated with 9 J/cm^2, the total percentage of apoptosis increased to around 37.84%, with a more significant occurrence of early apoptosis (28.88%).

To obtain more information concerning the involvement of apoptosis, the biochemical features were analyzed with TUNEL assay. SCC-13 cells were incubated with RF or RFTA (50 μM) for 3 h, irradiated with 9 J/cm^2 and then incubated for an additional 24 h. The results showed that in RF and RFTA-stimulated cells, this index was 6.14% and 8.67% respectively (Fig. 3B). These data may indicate that RFTA exhibited a higher capacity for stimulating apoptosis compared to RF, regardless of the light intensity.

The expression of Bax, Bcl-2 and procaspase-3, proteins related to apoptosis, was also analyzed by immunoblotting. As shown in Fig. 3(D–E), the treatments with RFTA decreased the expression of procaspase-3 ($p < 0.05$) and inhibited the expression of the antiapoptotic protein Bcl-2, compared to controls ($p < 0.05$). However, the expression of Bax did not exhibit a significant variation after PDT.

3.4. Intracellular Reactive Species Production After PDT

The analysis of DCF-DA fluorescence intensity showed that control cells irradiated with 4.5 or 9 J/cm^2 light doses did not exhibit any increase in the intracellular reactive species (RS) levels. Nevertheless, ROS production rose in the presence of both Ps, compared to control, when cells were exposed to the 9 J/cm^2 dose (Fig. 4A). Moreover, there was a significant Ps-light intensity interaction [$F_{4,18} = 4.07$; $p = 0.0159$], indicating that the effects of the compounds on ROS generation

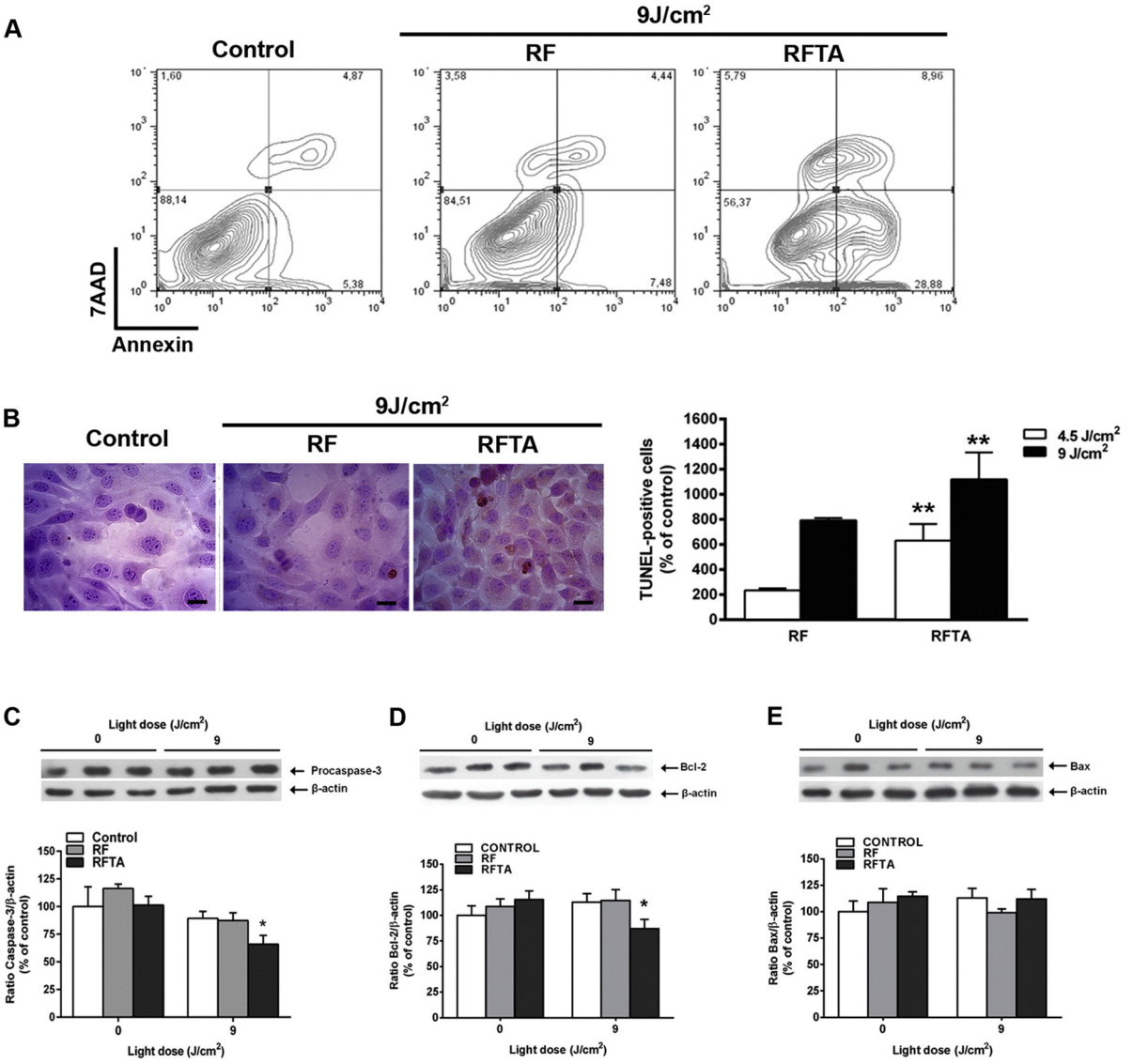

Fig. 3. SCC-13 cell death mechanism induced by photosensitizers with or without irradiation. (A) Flow cytometry contour plots of annexin V-PE/7AAD stained SCC-13 cells. The lower left quadrant (PE-A−/7AAD−) represents viable cells, while the lower right (PE-A+/7AAD−) and upper right (PE-A+/7AAD+) quadrants show apoptotic and necrotic cells and late apoptotic cells, respectively. (B) Representative microphotograph and TUNEL-positive cell quantification (nucleus in brown; scale bar: 8 μm.). Data are expressed as number of TUNEL-positive cells (% of control: absence of PS and light exposure) and shown as mean ± S.E.M. Two-way ANOVA, treatment (RF vs. RFTA) [$F_{1,11} = 11.95$; $p = 0.0054$]; as well as a significant [$F_{1,11} = 5.69$; $p = 0.036$] main effect of light intensity (4.5 vs. 9.0 J/cm^2), Bonferroni post-hoc test: $^{**}p < 0.01$. (C, D, E) Representative blots of the changes in the expression of cell death markers (caspase-3, Bcl-2 and Bax) when cells were treated with RF and RFTA photodynamic treatment (9 J/cm^2). The β-actin was used as loading control. $^{*}p < 0.05$ indicates the statistical difference from controls by two-way ANOVA, followed by Tukey post-hoc test. (For interpretation of the references to color in this figure legend, the reader is referred to the web version of this article.)

depended on the light intensity, indicating significant differences compared to control at the same light intensity.

As PDT produced an increase in RS levels, the cytoplasmic $\bullet O_2^-$ levels were evaluated using the redox-sensitive fluorescent probe DHE. A significant rise in $\bullet O_2^-$ generation, 6 h after PDT, was observed compared to irradiated cells without Ps and to treated cells with Ps in darkness (Fig. 4B). Furthermore, there was a significant Ps-light intensity interaction [$F_{2,30} = 15.11$; $p < 0.0001$], indicating that the effects of the compounds on $\bullet O_2^-$ generation depended on the light intensity.

In addition, in order to evaluate if the reactive oxygen species could be involved in the decrease of cell viability, the antioxidant Trolox (20 μM) was used. The results obtained showed that the percentage of viable SCC-13 cells pre-treated with Trolox was higher than in cells treated with PDT without the antioxidant (Fig. 4C).

3.5. Cell Death Induced by RFTA-PDT Involves the Activation of ERK 1/2 Protein Kinase

The above results indicated that RFTA-PDT induced cell death by increasing the intracellular ROS levels. Moreover, it is well known that reactive oxygen species are capable of inducing MAPK activation in different cell types [35,36]. Therefore, to investigate whether the activation of ERK 1/2 and $p38^{MAPK}$ may have been involved in apoptosis induced by RFTA-PDT, the phosphorylated and total form of ERK 1/2 and $p38^{MAPK}$ were analyzed by Western blotting. Although the phosphorylation of $p38^{MAPK}$ did not exhibit a significant interaction between Ps and irradiation (Fig. 5A), a significant increase in phosphorylated ERK 1/2 ($p < 0.05$) was detected in cells treated with RF and RFTA after light irradiation (9 J/cm^2) (Fig. 5B).

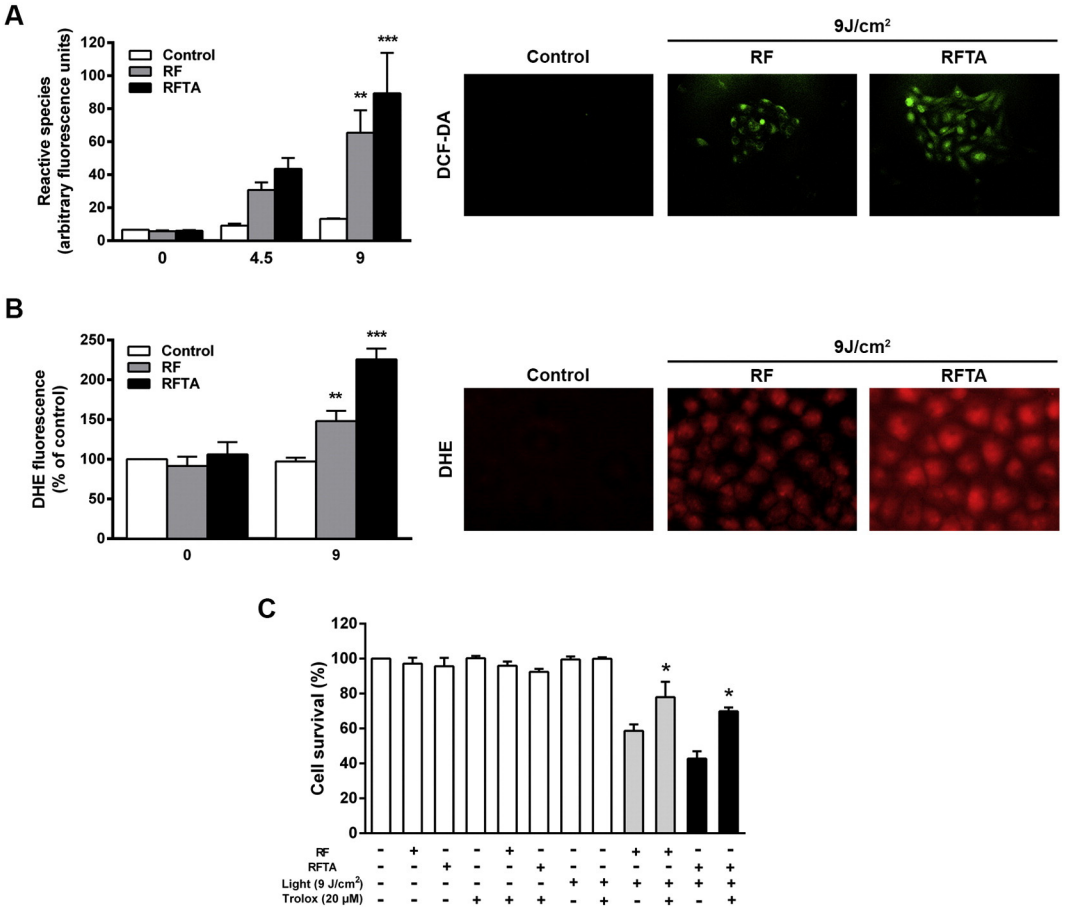

Fig. 4. Reactive species production in SCC-13 cells mediated by photosensitizers with or without irradiation. (A) Representative microphotograph and measurement of DCF-DA fluorescence intensity after PDT in SCC-13 cells after treatment with RF or RFTA and irradiation using different blue light doses (4.5 or 9 J/cm^2). Two-way ANOVA, control vs. RF vs. RFTA [$F_{2,18} = 10.99$; $p = 0.0008$], as well as effect of light intensity: 0 vs. 4.5 vs. 9.0 J/cm^2, [$F_{2,18} = 19.75$; $p < 0.0001$]. Bonferroni post-hoc test: $^{**}p < 0.01$ and $^{***}p < 0.001$ vs. control at the same light intensity condition. (B) Representative microphotograph and quantification of DHE fluorescence intensity after PDT. Two-way ANOVA, control vs. RF vs. RFTA [$F_{2,30} = 19.2$; $p < 0.0001$], as well as effect of light intensity: 0 vs. 4.5 vs. 9.0 J/cm^2, [$F_{1,30}$ 40.34; $p < 0.0001$]. Bonferroni post-hoc test: $^{**}p < 0.01$ and $^{***}p < 0.001$ vs. control at the same light intensity condition. Data are expressed as number of arbitrary fluorescence units, % of control and expressed as mean ± S.E.M. (C) Cell survival after PDT in Trolox pre-treated SCC-13 cells (20 μM). Data are represented as cell survival percentage of control and expressed as mean ± S.E.M. Student's t-test: $^{*}p < 0.05$, RF or RFTA with Trolox vs. RF or RFTA without Trolox at 9 J/cm^2. (For interpretation of the references to color in this figure legend, the reader is referred to the web version of this article.)

In addition, in order to analyze if the reactive oxygen species could be involved in the activation of ERK 1/2, the antioxidant Trolox (20 μM) was used. The incubation with Trolox partially inhibited the phosphorylation of ERK 1/2 in RF-PDT ($p = 0.042$ and $p = 0.0275$ respectively) and ERK 2 in RFTA-PDT ($p = 0.0262$) when compared to cells treated with PDT without the antioxidant (Fig. 5C). Next, taking into account that the ERK 1/2 could be participate in the cell death after PDT, a pre-treatment with the MEK inhibitor (PD 098059) was carried out. As shown in Fig. 5D, the cell viability after RF or RFTA-PDT with inhibitor remained similar to observed with PDT without inhibitor.

4. Discussion

Recently, significant research efforts have been focused on finding newer and more efficient photosensitizers for PDT. One of the critical steps to identify an efficient Ps for PDT is to determine its selectivity and capacity to accumulate in target cells [37]. The present study demonstrates the efficacy of the RF ester derivative, RFTA, as a photosensitizer in PDT which was able to induce cell death in squamous carcinoma cells (SCC-13), thus revealing apoptosis to be the primary type of cell death induced by ROS ($\bullet O_2^-$) production and likely to involve p-ERK 1/2 activation.

Although there have been very few investigations using RF in PDT to treat cancer [38], it has been selected as a Ps in other types of studies due to its photosensitizing properties [14,39,40]. However, since riboflavin is a hydrosoluble vitamin, it is poorly incorporated into cells. Thus we chose to analyze the effects of RFTA because of its higher incorporation in the SCC-13 cell line and its incapability to induce toxicity in darkness in the range of concentrations lower than 50 μM, as demonstrated in our experimental conditions.

Light sources for exciting photosensitizers, including laser, light-emitting diodes and many other types of visible light, play an important role in improving PDT efficacy. Ps may become activated by one or several types of light, as the optimal light effect depends on the excitation peaks of the photosensitizer drug used and the target tissue [8]. Another important characteristic of the light employed in PDT is its penetration into the tissue, which varies according to wavelength, with the depth of light penetration in the tissue increasing with longer wavelengths [41]. A specific wavelength (446 nm) in the visible spectrum, which is known to excite RF and RFTA, was used to photoactivate both Ps, and photoactivation with different energy densities. An important characteristic of a Ps in PDT is also its preferential accumulation in target tissues and the rapid clearance from normal tissues, thus maximizing the selectivity of therapy [7,42]. The Ps uptake by SCC-13 cells was higher than in normal keratinocytes cells, indicating that PDT with RF and RFTA could be effective for treating tumoral cells.

The light dose–response curve showed that the phototoxic effect on cells increased with light dose, being higher in SCC-13 than in HaCat cells, suggesting that tumoral cells were more sensitive to PDT. It was noteworthy that in the RFTA treatment, the phototoxic effect was

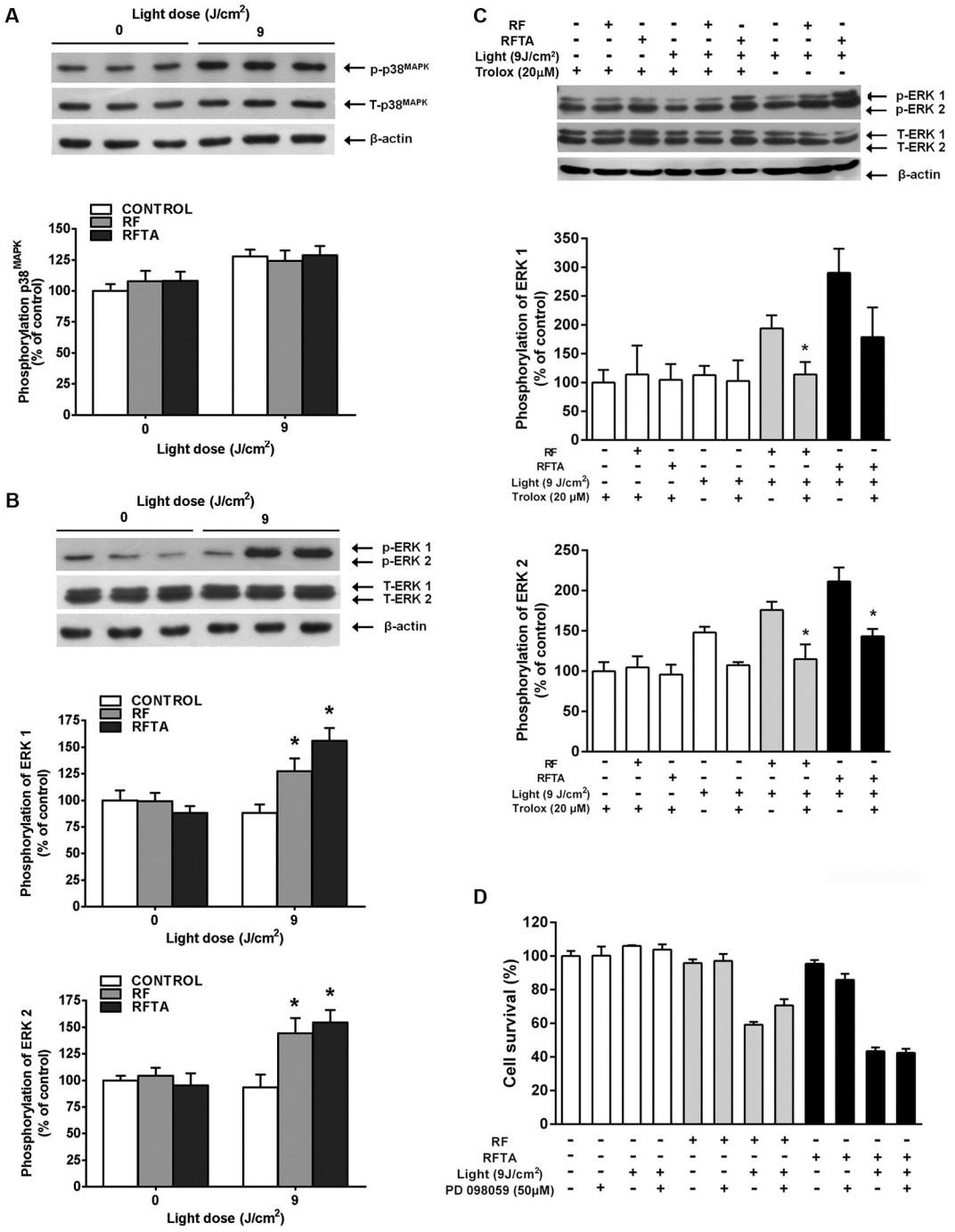

Fig. 5. Phosphorylated p38^{MAPK} and ERK 1/2 protein expression analysis in SCC-13 cells mediated by photosensitizers with or without irradiation. (A) Representative blot of immunoreactivity of phospho-p38^{MAPK}, total-p38^{MAPK} in SCC-13 cells treated with RF and RFTA alone or irradiated with 9 J/cm^2. (B and C) Representative blot of phospho-ERK 1, total-ERK 1, phospho-ERK 2, total-ERK 2 immunoreactivity in SCC-13 cells with or without Trolox exposition (20 μM). The phosphorylated level was determined by computer-assisted densiometry as a ratio of the O.D. of the phosphorylated band and the O.D. of the total band, with the data being expressed as percentage of the control. β-Actin was used as the control for loading. Two-way ANOVA, following by Tukey post-hoc test: *$p < 0.05$ vs. control at the same light intensity condition without Trolox. Student's t-test: *$p < 0.05$, RF or RFTA with Trolox vs. RF or RFTA without Trolox at 9 J/cm^2. (D) Cell survival after PDT in PD 098059 pre-treated SCC-13 cells (50 μM). Data are represented as cell survival percentage of control and expressed as mean ± S.E.M.

greater at the highest light dose compared with RF. Furthermore, it has been previously described that RF is susceptible to photodegradation, while RFTA is substantially more photostable than RF, since the half-life of RFTA photodegradation is ~30 times longer than that of RF [20]. Despite RFTA and RF being able to absorb light at nearly the same rate, RFTA might be more efficient than RF as a photosensitizer in PDT for superficial skin diseases, as this wavelength presents a low penetration in the tissue [41].

PDT can induce cell death in culture through several mechanisms [21,22]. In this investigation, irradiated RF and RFTA induced cell death mainly by an apoptotic mechanism in the SCC-13 cells, revealed by the characteristic condensation of the chromatin. Moreover, the increased phosphatidylserine externalization and higher number of TUNEL-positive cell, after RFTA-PDT confirmed the occurrence of apoptotic cell death. This treatment also generated ultrastructural changes similar to those described for cells undergoing apoptosis, including

chromatin condensation, cell and nuclear shrinkage and membrane blebbing [24].

In general, the activation of caspase pathways is essential to produce apoptotic morphological and biochemical changes [43]. Therefore, to investigate further the mechanisms involved in RFTA-PDT induced apoptosis in SCC-13 cells, we examined the expression of the procaspase-3, Bcl-2 and Bax proteins in a caspase-dependent pathway by Western blot. The decreased expression of procaspase-3 and Bcl-2 in RFTA-PDT treated-cells led us to speculate that the down regulation of these molecules could have been responsible for the occurrence of the apoptosis observed. Unexpectedly, the expression of Bax was not modified in these tumoral cells after PDT when compared to control cells, as reported in other studies [44,45]. Moreover, a possible contribution of additional proapoptotic molecules cannot be discarded in this process, as described by other investigators [46,47]. In our study, when the light dose was increased to 18 J/cm^2 in cells treated with RFTA, cell death was induced through events related to the necrotic morphology, which involved rupture of the plasma membrane with the subsequent release of cytoplasmic constituents and the absence of chromatin condensation [48]. Based in these results it is possible to postulate that an efficient induction of apoptosis in vivo by tissue irradiation after RFTA administration should be carried out with low light doses, thereby preventing the stimulation of the immune system or induction of antitumor immune reactions that occur when necrosis is induced [24].

When activated photosensitizers transfer energy to molecular oxygen, they generate ROS, which interact with biologic substrates triggering different cellular responses. Some studies have reported that overproduction of ROS causes cell damage and promotes not only necrosis, but can also activate signaling pathways involved in apoptosis [49–51]. Consequently, to evaluate whether the generation of intracellular ROS could be involved in the mechanism of cell death, we employed DCF-DA and DHE. It has been reported that the light exposure of RF in the presence of molecular oxygen can generate ROS strong enough to elicit toxic insults or injuries, leading to photodamage and even cell death [13,14]. Although, ROS levels were increased in the SCC-13 cells treated by PDT, this response was higher in RFTA-treated cells, suggesting that this Ps could be potentially used as an efficient generator of intracellular ROS, such as $^{\bullet}O_2^-$. Based on these results and in an attempt to confirm the involvement of ROS in cell viability, the antioxidant Trolox was used before PDT application. These results supported the contribution of ROS production in increasing SCC-13 cell death. Related to this, the photoactivation of Ps derivatives has been described in ROS formations, which act as primary messengers that trigger multiple signaling pathways leading to cell death [52].

The mechanisms involved in programmed cell death induced by PDT could be related to the activation of MAPKs [53]. In fact, it is known that MAPKs play important roles in a variety of cellular processes, such as cell proliferation and apoptosis [54], and it has been demonstrated that ROS can induce the activation of p38^{MAPK} pathways in various cell models, causing cell death in several cell types [52,55,56]. Although, in the present study, PDT with RF and RFTA increased the ROS levels, the p38^{MAPK} phosphorylation was unchanged in treated cells, suggesting no direct relationship between compound exposure and irradiation with the modulation of p38^{MAPK} activity in SCC-13 cells. Moreover, it has been reported that ERK 1/2, one of the more ubiquitous signaling enzymes, activated in response to anticancer compounds such as cisplatin, piperlongumine and by ROS playing role in the mechanism of cell death [57,58].

In line with this previous report, our results indicate that ERK 1/2 activation, observed after PDT, may be due an increment of intracellular ROS levels, since after employing the antioxidant Trolox it was observed a partial inhibition of ERK 1/2 phosphorylation in response to PDT. It has been recognized that antioxidants can attenuate MAPK–ERK activation, suggesting that ROS may modulate these kinases [59]. In addition, aiming to analyze the involvement of ERK phosphorylation in the PDT-induced cell death we employed the MEK inhibitor PD 098059. Under our experimental conditions, the pre-treatment with MEK inhibitor did not induce changes in SCC-13 cell survival, suggesting that ERK 1/2 phosphorylation represents a consequence of exposure to RFTA + light, but that this event does not necessarily represent the cause of cell viability loss. Noteworthy, there are studies in others cells types showing ERK activation as mechanism of protection from apoptotic death after oxidative stress [60,61] as well as ERK activation involved in the mechanism of cell death [57,58]. However, our result indicates that ERK 1/2 activation was not associated with either cellular damage induced by PDT or some protective mechanism.

In summary, our study demonstrates that RFTA trigger apoptosis in SCC-13 cells after visible light irradiation (9 J/cm^2) and suggests that ROS ($^{\bullet}O_2^-$) production might be involved in this effect. It is worth noting that this postulated mechanism might provide significant insights into RFTA-PDT and lead to new therapeutic strategies to treat proliferative superficial skin diseases in vivo. Furthermore, as this mechanism was not associated with necrosis, thus avoiding inflammation and damage do not affect the surrounding healthy tissue.

Acknowledgments

We are especially grateful to Mrs. María Elena Pereyra, Mrs. Lucía Artino, Eng. Néstor Boetto and PhD Ernesto Haggi for their technical assistance and to native speaker Dr. Paul Hobson for revising the manuscript. This work was supported by grants from Secretaría de Ciencia y Tecnología, Universidad Nacional de Córdoba (SECYT RR N° 203/14) and from CAPES/MINCyT no. 249/14.

References

[1] R.M. Szeimies, C.A. Morton, A. Sidoroff, L.R. Braathen, Photodynamic therapy for non-melanoma skin cancer, Acta Derm. Venereol. 85 (2005) 483–490.
[2] A. Juarranz, P. Jaen, F. Sanz-Rodriguez, J. Cuevas, S. Gonzalez, Photodynamic therapy of cancer. Basic principles and applications, Clin. Transl. Oncol. 10 (2008) 148–154.
[3] D. Nowis, M. Makowski, T. Stoklosa, M. Legat, T. Issat, J. Golab, Direct tumor damage mechanisms of photodynamic therapy, Acta Biochim. Pol. 52 (2005) 339–352.
[4] N.L. Oleinick, R.L. Morris, I. Belichenko, The role of apoptosis in response to photodynamic therapy: what, where, why, and how, Photochem. Photobiol. Sci. 1 (2002) 1–21.
[5] R.D. Almeida, B.J. Manadas, A.P. Carvalho, C.B. Duarte, Intracellular signaling mechanisms in photodynamic therapy, Biochim. Biophys. Acta 1704 (2004) 59–86.
[6] L. Wyld, M.W. Reed, N.J. Brown, Differential cell death response to photodynamic therapy is dependent on dose and cell type, Br. J. Cancer 84 (2001) 1384–1386.
[7] P. Agostinis, K. Berg, K.A. Cengel, T.H. Foster, A.W. Girotti, S.O. Gollnick, S.M. Hahn, M.R. Hamblin, A. Juzeniene, D. Kessel, M. Korbelik, J. Moan, P. Mroz, D. Nowis, J. Piette, B.C. Wilson, J. Golab, Photodynamic therapy of cancer: an update, CA Cancer J. Clin. 61 (2011) 250–281.
[8] L.R. Braathen, R.M. Szeimies, N. Basset-Seguin, R. Bissonnette, P. Foley, D. Pariser, R. Roelandts, A.M. Wennberg, C.A. Morton, D. International Society for Photodynamic Therapy in, Guidelines on the use of photodynamic therapy for nonmelanoma skin cancer: an international consensus. International Society for Photodynamic Therapy in Dermatology, J. Am. Acad. Dermatol. 56 (2007) (2005) 125–143.
[9] M. Wainwright, Photodynamic therapy: the development of new photosensitisers, Anti Cancer Agents Med. Chem. 8 (2008) 280–291.
[10] A.R. Soares, M.G. Neves, A.C. Tome, M.C. Iglesias-de la Cruz, A. Zamarron, E. Carrasco, S. Gonzalez, J.A. Cavaleiro, T. Torres, D.M. Guldi, A. Juarranz, Glycophthalocyanines as photosensitizers for triggering mitotic catastrophe and apoptosis in cancer cells, Chem. Res. Toxicol. 25 (2012) 940–951.
[11] V. Massey, The chemical and biological versatility of riboflavin, Biochem. Soc. Trans. 28 (2000) 283–296.
[12] A.M. Edwards, E. Silva, Effect of visible light on selected enzymes, vitamins and amino acids, J. Photochem. Photobiol. B 63 (2001) 126–131.
[13] M.M. Jazzar, I. Naseem, Genotoxicity of photoilluminated riboflavin in the presence of Cu(II), Free Radic. Biol. Med. 21 (1996) 7–14.
[14] E. Husain, I. Naseem, Riboflavin-mediated cellular photoinhibition of cisplatin-induced oxidative DNA breakage in mice epidermal keratinocytes, Photodermatol. Photoimmunol. Photomed. 24 (2008) 301–307.
[15] M.A. Munoz, A. Pacheco, M.I. Becker, E. Silva, R. Ebensperger, A.M. Garcia, A.E. De Ioannes, A.M. Edwards, Different cell death mechanisms are induced by a hydrophobic flavin in human tumor cells after visible light irradiation, J. Photochem. Photobiol. B 103 (2011) 57–67.
[16] K. Sato, N. Sakakibara, K. Hasegawa, H. Minami, T. Tsuji, A preliminary report of the treatment of blue nevus with dermal injection of riboflavin and exposure to near-ultraviolet/visible radiation (ribophototherapy), J. Dermatol. Sci. 23 (2000) 22–26.
[17] H.T. Yang, P.C. Chao, M.C. Yin, Riboflavin at high doses enhances lung cancer cell proliferation, invasion, and migration, J. Food Sci. 78 (2013) H343–H349.

[18] A.H. Chaves Neto, K.J. Pelizzaro-Rocha, M.N. Fernandes, C.V. Ferreira-Halder, Antitumor activity of irradiated riboflavin on human renal carcinoma cell line 786-O, Tumour Biol.J. Int. Soc. Oncodev. Biol. Med. 36 (2015) 595–604.
[19] A.M. Edwards, C. Bueno, A. Saldano, E. Silva, K. Kassab, L. Polo, G. Jori, Photochemical and pharmacokinetic properties of selected flavins, J. Photochem. Photobiol. B 48 (1999) 36–41.
[20] C.K. Remucal, K. McNeill, Photosensitized amino acid degradation in the presence of riboflavin and its derivatives, Environ. Sci. Technol. 45 (2011) 5230–5237.
[21] E. Buytaert, G. Callewaert, J.R. Vandenheede, P. Agostinis, Deficiency in apoptotic effectors Bax and Bak reveals an autophagic cell death pathway initiated by photodamage to the endoplasmic reticulum, Autophagy 2 (2006) 238–240.
[22] M. Dewaele, T. Verfaillie, W. Martinet, P. Agostinis, Death and survival signals in photodynamic therapy, Methods Mol. Biol. 635 (2010) 7–33.
[23] G. Kroemer, L. Galluzzi, P. Vandenabeele, J. Abrams, E.S. Alnemri, E.H. Baehrecke, M.V. Blagosklonny, W.S. El-Deiry, P. Golstein, D.R. Green, M. Hengartner, R.A. Knight, S. Kumar, S.A. Lipton, W. Malorni, G. Nunez, M.E. Peter, J. Tschopp, J. Yuan, M. Piacentini, B. Zhivotovsky, G. Melino, Classification of cell death: recommendations of the Nomenclature Committee on Cell Death 2009, Cell Death Differ. 16 (2009) 3–11.
[24] N. Vanlangenakker, T. Vanden Berghe, D.V. Krysko, N. Festjens, P. Vandenabeele, Molecular mechanisms and pathophysiology of necrotic cell death, Curr.Mol. Med. 8 (2008) 207–220.
[25] J. Hitomi, D.E. Christofferson, A. Ng, J. Yao, A. Degterev, R.J. Xavier, J. Yuan, Identification of a molecular signaling network that regulates a cellular necrotic cell death pathway, Cell 135 (2008) 1311–1323.
[26] S. Ichinose, J. Usuda, T. Hirata, T. Inoue, K. Ohtani, S. Maehara, M. Kubota, K. Imai, Y. Tsunoda, Y. Kuroiwa, K. Yamada, H. Tsutsui, K. Furukawa, T. Okunaka, N.L. Oleinick, H. Kato, Lysosomal cathepsin initiates apoptosis, which is regulated by photodamage to Bcl-2 at mitochondria in photodynamic therapy using a novel photosensitizer, ATX-s10 (Na), Int. J. Oncol. 29 (2006) 349–355.
[27] T. Kriska, W. Korytowski, A.W. Girotti, Role of mitochondrial cardiolipin peroxidation in apoptotic photokilling of 5-aminolevulinate-treated tumor cells, Arch. Biochem. Biophys. 433 (2005) 435–446.
[28] Y. Liu, E.G. Shepherd, L.D. Nelin, MAPK phosphatases—regulating the immune response, Nat. Rev. Immunol. 7 (2007) 202–212.
[29] H.T. Ji, L.T. Chien, Y.H. Lin, H.F. Chien, C.T. Chen, 5-ALA mediated photodynamic therapy induces autophagic cell death via AMP-activated protein kinase, Mol. Cancer 9 (2010) 91.
[30] R. Bhowmick, A.W. Girotti, Signaling events in apoptotic photokilling of 5-aminolevulinic acid-treated tumor cells: inhibitory effects of nitric oxide, Free Radic. Biol. Med. 47 (2009) 731–740.
[31] F.K. Ogasawara, Y. Wang, D.R. Bobbitt, Dynamically modified, biospecific optical fiber sensor for riboflavin binding protein based on hydrophobically associated 3-octylriboflavin, Anal. Chem. 64 (1992) 1637–1642.
[32] J.G. Rheinwald, M.A. Beckett, Tumorigenic keratinocyte lines requiring anchorage and fibroblast support cultures from human squamous cell carcinomas, Cancer Res. 41 (1981) 1657–1663.
[33] R.B. Leal, F.M. Cordova, L. Herd, L. Bobrovskaya, P.R. Dunkley, Lead-stimulated p38MAPK-dependent Hsp27 phosphorylation, Toxicol. Appl. Pharmacol. 178 (2002) 44–51.
[34] V.P. Bindokas, J. Jordan, C.C. Lee, R.J. Miller, Superoxide production in rat hippocampal neurons: selective imaging with hydroethidine, J. Neurosci. 16 (1996) 1324–1336.
[35] P.V. Usatyuk, S. Vepa, T. Watkins, D. He, N.L. Parinandi, V. Natarajan, Redox regulation of reactive oxygen species-induced p38 MAP kinase activation and barrier dysfunction in lung microvascular endothelial cells, Antioxid. Redox Signal. 5 (2003) 723–730.
[36] L. Conde de la Rosa, M.H. Schoemaker, T.E. Vrenken, M. Buist-Homan, R. Havinga, P.L. Jansen, H. Moshage, Superoxide anions and hydrogen peroxide induce hepatocyte death by different mechanisms: involvement of JNK and ERK MAP kinases, J. Hepatol. 44 (2006) 918–929.
[37] I. Yoon, J.Z. Li, Y.K. Shim, Advance in photosensitizers and light delivery for photodynamic therapy, Clin. Endosc. 46 (2013) 7–23.
[38] I. Hassan, S. Chibber, I. Naseem, Vitamin B(2): a promising adjuvant in cisplatin based chemoradiotherapy by cellular redox management, Food Chem. Toxicol. 59 (2013) 715–723.
[39] I. Hassan, S. Chibber, I. Naseem, Ameliorative effect of riboflavin on the cisplatin induced nephrotoxicity and hepatotoxicity under photoillumination, Food Chem. Toxicol. 48 (2010) 2052–2058.
[40] A.C. de Souza, L. Kodach, F.R. Gadelha, C.L. Bos, A.D. Cavagis, H. Aoyama, M.P. Peppelenbosch, C.V. Ferreira, A promising action of riboflavin as a mediator of leukaemia cell death, Apoptosis 11 (2006) 1761–1771.
[41] B.W. Henderson, T.J. Dougherty, How does photodynamic therapy work? Photochem. Photobiol. 55 (1992) 145–157.
[42] R.R. Allison, C.H. Sibata, Oncologic photodynamic therapy photosensitizers: a clinical review, Photodiagn. Photodyn. Ther. 7 (2010) 61–75.
[43] N.A. Thornberry, Y. Lazebnik, Caspases: enemies within, Science 281 (1998) 1312–1316.
[44] T. Liu, B. Hannafon, L. Gill, W. Kelly, D. Benbrook, Flex-Hets differentially induce apoptosis in cancer over normal cells by directly targeting mitochondria, Mol. Cancer Ther. 6 (2007) 1814–1822.
[45] A.M. Saleh, M.M. El-Abadelah, M.A. Aziz, M.O. Taha, A. Nasr, S.A. Rizvi, Antiproliferative activity of the isoindigo 5′-Br in HL-60 cells is mediated by apoptosis, dysregulation of mitochondrial functions and arresting cell cycle at G0/G1 phase, Cancer Lett. 361 (2015) 251–261.
[46] J.C. Sharpe, D. Arnoult, R.J. Youle, Control of mitochondrial permeability by Bcl-2 family members, Biochim. Biophys. Acta 1644 (2004) 107–113.
[47] M. Forte, P. Bernardi, The permeability transition and BCL-2 family proteins in apoptosis: co-conspirators or independent agents? Cell Death Differ. 13 (2006) 1287–1290.
[48] S.Y. Proskuryakov, A.G. Konoplyannikov, V.L. Gabai, Necrosis: a specific form of programmed cell death? Exp. Cell Res. 283 (2003) 1–16.
[49] S.B. Wallach-Dayan, G. Izbicki, P.Y. Cohen, R. Gerstl-Golan, A. Fine, R. Breuer, Bleomycin initiates apoptosis of lung epithelial cells by ROS but not by Fas/FasL pathway, Am. J. Physiol. Lung Cell. Mol. Physiol. 290 (2006) L790–L796.
[50] H. Kolarova, R. Bajgar, K. Tomankova, E. Krestyn, L. Dolezal, J. Halek, In vitro study of reactive oxygen species production during photodynamic therapy in ultrasound-pretreated cancer cells, Physiol. Res. 56 (Suppl 1) (2007) S27–S32.
[51] M.L. Circu, T.Y. Aw, Reactive oxygen species, cellular redox systems, and apoptosis, Free Radic. Biol. Med. 48 (2010) 749–762.
[52] I. Moserova, J. Kralova, Role of ER stress response in photodynamic therapy: ROS generated in different subcellular compartments trigger diverse cell death pathways, PLoS One 7 (2012), e32972.
[53] A. Casas, G. Di Venosa, T. Hasan, B. Al, Mechanisms of resistance to photodynamic therapy, Curr. Med. Chem. 18 (2011) 2486–2515.
[54] S. Cagnol, J.C. Chambard, ERK and cell death: mechanisms of ERK-induced cell death—apoptosis, autophagy and senescence, FEBS J. 277 (2010) 2–21.
[55] B.S. Pan, Y.K. Wang, M.S. Lai, Y.F. Mu, B.M. Huang, Cordycepin induced MA-10 mouse leydig tumor cell apoptosis by regulating p38 MAPKs and PI3K/AKT signaling pathways, Sci. Rep. 5 (2015) 13372.
[56] T.H. Ho-Bouldoires, A. Claperon, M. Mergey, D. Wendum, C. Desbois-Mouthon, S. Tahraoui, L. Fartoux, H. Chettouh, F. Merabtene, O. Scatton, M. Gaestel, F. Praz, C. Housset, L. Fouassier, Mitogen-activated protein kinase-activated protein kinase 2 mediates resistance to hydrogen peroxide-induced oxidative stress in human hepatobiliary cancer cells, Free Radic. Biol. Med. (2015).
[57] H. Randhawa, K. Kibble, H. Zeng, M.P. Moyer, K.M. Reindl, Activation of ERK signaling and induction of colon cancer cell death by piperlongumine, Toxicol. in Vitro 27 (2013) 1626–1633.
[58] W.J. Lee, M. Hsiao, J.L. Chang, S.F. Yang, T.H. Tseng, C.W. Cheng, J.M. Chow, K.H. Lin, Y.W. Lin, C.C. Liu, L.M. Lee, M.H. Chien, Quercetin induces mitochondrial-derived apoptosis via reactive oxygen species-mediated ERK activation in HL-60 leukemia cells and xenograft, Arch. Toxicol. 89 (2015) 1103–1117.
[59] A. Gupta, S.F. Rosenberger, G.T. Bowden, Increased ROS levels contribute to elevated transcription factor and MAP kinase activities in malignantly progressed mouse keratinocyte cell lines, Carcinogenesis 20 (1999) 2063–2073.
[60] R. Aikawa, I. Komuro, T. Yamazaki, Y. Zou, S. Kudoh, M. Tanaka, I. Shiojima, Y. Hiroi, Y. Yazaki, Oxidative stress activates extracellular signal-regulated kinases through Src and Ras in cultured cardiac myocytes of neonatal rats, J. Clin. Invest. 100 (1997) 1813–1821.
[61] X. Wang, J.L. Martindale, Y. Liu, N.J. Holbrook, The cellular response to oxidative stress: influences of mitogen-activated protein kinase signalling pathways on cell survival, Biochem. J. 333 (Pt 2) (1998) 291–300.